Jerome P. Charba*
Meteorological Development Laboratory
Office of Science and Technology
National Weather Service, NOAA
Silver Spring, Maryland

Feng Liang
Beijing Meteorological Bureau
Beijing, 100089, China

1. INTRODUCTION

The Meteorological Development Laboratory (MDL) is developing a statistically-based system for short range thunderstorm forecasts (Charba and Feng 2005). Specifically, the forecasts are for the occurrence of one or more cloud-to-ground (CTG) lightning strikes in 20-km gridboxes in 2-h periods out to 24 hours. This gridded product shares some features with a suite of station-oriented aviation weather products from MDL's new Local Aviation MOS Program (LAMP) (Ghirardelli 2005). Because the LAMP thunderstorm product involves frequent (hourly) updates of MOS thunderstorm forecasts, it makes heavy use of high resolution observational data types. Two key data types are CTG strikes from the upgraded National Lightning Detection Network (NLDN) (Cummins et al. 1998) and digital radar reflectivities from the Weather Surveillance Radar 1988 (Doppler) (WSR-88D) (Fread et al. 1995).

Since the LAMP thunderstorm product is entirely automated, the input data must have high quality. Studies of CTG lightning data from the upgraded NLDN (Cummins et al. 1998; Idone et al. 1998 a,b) indicate a positioning accuracy within 500 m and a detection efficiency (percentage of actual strikes) of 80-90 % for all but very weak strikes. This quality level is quite sufficient for the LAMP product and probably most other forecasting applications. MDL has acquired, from the Global Hydrology Resource Center (GHRC) in Huntsville, Alabama, an archive of strike data for the period April 1994 to the present.

---

 * *Corresponding author address:*
Dr. Jerome P. Charba, National Weather Service
1325 East West Highway, Room 10410
Silver Spring, MD 20910-3283
email: jerome.charba@noaa.gov

An inherent aspect of radar reflectivity measurements is the presence of error and non-precipitation echoes. In fact, the need for removal of stationary non-precipitation echoes, such as ground clutter (GC) and anomalous propagation (AP), is so great that automated screening procedures to reduce their occurrence are integral part of the WSR-88D data acquisition system. For some applications of the reflectivities, such as precipitation estimation, additional quality control procedures that further attempt to remove non-precipitation echoes are applied (Fulton et al. 1998). However, even these miss some types of unwanted echoes, and some applications of the reflectivities do not incorporate them.

2. RADAR DATA PROPERTIES, PRE-PROCESSING, AND PREVIOUS QUALITY CONTROL

Two gridded radar reflectivity products with contiguous United States (CONUS) coverage were available for development and implementation of the LAMP thunderstorm product. One product, which is produced in real time by Weather Science Incorporated (WSI), consists of latitude-longitude reflectivity grids with a mesh of about 2 km. The grids depict reflectivity in 16 categories (Table 1), and they are produced and archived four times per hour. The nominal time stamps are :00, :15, :30, and :45, but the reflectivity measurements are taken over a 5-10 min interval preceeding these times. Graphical displays of current grids can be viewed at http://www.intellicast.com/. MDL has obtained an archive of these grids (from GHRC) for the period 1 April 1997 to 31 March 2002.

Another gridded national reflectivity product prepared in real time is a composite of local grids extracted from Radar Coded Messages (RCMs) (OFCM 1991; Kitzmiller et al. 2002). Each local grid has a meshlength of 10 km and the coverage applies to a single WSR-88D radar. A gridbox con-

tains the maximum reflectivity falling within it based on 1 deg azimuth X 1 km range "sectorized hybrid scan" reflectivities (Fulton et al. 1998). The RCM reflectivities are represented in seven categories, which match the WSI categories in the mid-range, but span 2-4 WSI categories at low and high reflectivities (Table 1). The RCM grids are produced twice per hour for the nominal times :15 and :45. Graphical displays of current grids can be viewed at http://iwin.nws.noaa.gov/iwin/images/rcm.html. For application in this study, an archive of the national RCM reflectivity grids begins 1 April 2002 for the :15 nominal time, and the corresponding :45 archive begins 1 June 2003; the archive for both times extends to the present.

Table 1. WSI and RCM radar reflectivity categories and ranges.

WSI category	RCM category	Reflectivity range (dBZ)
0	0	0 – 4
1	0	5 – 9
2	0	10 – 14
3	1	15 – 19
4	1	20 – 24
5	1	25 – 29
6	2	30 – 34
7	2	35 – 39
8	3	40 – 44
9	4	45 – 49
10	5	50 – 54
11	6	55 – 59
12	6	60 – 64
13	6	65 – 69
14	6	70 – 74
15	6	≥ 75

Since development of the LAMP thunderstorm product required application of the archived WSI and RCM reflectivity data as a single historical dataset, it was essential to build as much consistency between them as possible. Also, since only the RCM data are available in real time to support operational implementation of products such as that of concern here, the archived WSI data were transformed to mimic the RCM product. Several procedures were applied to the WSI 2-km grids in this regard. One procedure consisted of their transferal ("interpolation") to the CONUS RCM 10-km grid (actually a very slightly expanded version). The interpolation involved assigning the highest WSI 2-km reflectivity to a 10-km RCM gridbox. Another consistency procedure is the application of an occultation grid (Kitzmiller et al. 2002), which identifies 10-km boxes with substantial radar beam blockage. The final procedure is the application of radar site "meta-data" (indicates the operational status of each radar). The meta-data are used to determine the distance of a 10-km gridbox to the nearest operating radar. If the gridbox ex-

hibits either beam blockage or lies beyond 230 km from the closest radar, missing is assigned when the inscribed 2-km WSI reflectivties are ≤ 4 dBZ (category 0); otherwise the highest reflectivity is assigned as usual. Note that the last two procedures should enhance the quality of the WSI 10-km reflectivity grids.

The quality control (QC) incorporated into the RCM reflectivity mosaics is entirely automated (and rather extensive). First, the local RCM grids embody the multiple QC procedures that characterize the WSR-88D hybrid scan reflectivity product (Fulton et al. 1998) since they are derived from this product (OFCM 1991). Specifically, these procedures correct the multi-tilt, volume scan reflectivities for partial beam obstruction and remove small non-precipitation and obvious AP echoes. Second, automated QC procedures are applied during construction of the CONUS RCM mosaic (Kitzmiller et al. 2002) to remove (1) low reflectivity echoes from migratory birds and insects, (2) non-precipitation echoes based on consistency checks with satellite-observed clouds and numerical model forecasts of atmospheric moisture/convective instability, and (3) residual echoes based on spatial continuity checks.

The QC incorporated into the WSI reflectivity data is not formally documented, but D. Callahan of WSI furnished pertinent information in a February 2004 email. He stated the original 2-km grids are generated from multi-tilt, volumetric scan reflectivities from WSR-88D radars. He also mentioned WSI application of terrain blockage masks associated with the hybrid scan processing and to the application of other automated and human consistency checks developed at WSI.

3. NON-PRECIPITATION ECHOES IN THE REFLECTIVITY GRIDS

Because it was not clear whether the QC built into the WSI and RCM 10-km reflectivity grids was sufficient for their direct input into the LAMP lightning product, an investigation of quality was performed. In the investigation, CTG lightning strikes were used as "ground truth" for (most) strong precipitation echoes, which is probably a safe assumption given the known high quality of these lightning data. However, it was first necessary to factor out short, undocumented gaps in the otherwise continuous CTG lightning data stream. For the period April 1994 – March 2005 gaps ascertained by the authors are listed in Table 2.

Table 2. Data gaps in the CTG lightning strike archive from the upgraded National Lightning Detection Network over the period April 1994 – March 2005.

Gap begins				Gap ends			
Year	Month	Day	Time (GMT)	Year	Month	Day	Time(GMT)
1994	07	31	0000	1994	07	31	2359
1996	09	01	0000	1996	09	01	2359
1997	06	05	0000	1997	06	05	1459
1997	06	14	0239	1997	06	14	0859
1997	07	12	1435	1997	07	12	1859
1997	10	12	0000	1997	10	13	2359
1998	07	31	2137	1998	07	31	2359
2000	05	27	0215	2000	05	27	2359
2001	08	02	0422	2001	08	02	2359
2003	08	18	0017	2003	08	18	2359

3.1 Lightning Relative Frequency Versus Radar Reflectivity

The initial examination of radar data quality consisted of statistical analysis of the relationship between CTG lightning relative frequency (LRF) and the concurrent radar reflectivity. For this analysis, a lightning event was defined as one or more CTG strikes in the 10-km radar gridbox over a 15-min period that begins 10 min before the radar nominal time and ends 5 min later. Experimentation with several other lightning-radar time configurations showed this one produced the best relationship. The analysis was conducted separately for the WSI and RCM archives because of the disparity in reflectivity (Table 1) and temporal resolution of the two products. Also, the archived data were divided into warm (April – September) and cool (October – March) seasons to segregate deep convective precipitation characterizing the former season from shallow stratiform precipitation that typifies the latter. In the derivation of the relationships, the data, for a given radar nominal time, were accumulated from all CONUS gridpoints with radar coverage (Fig. 1) and all hours of the day.

Fig. 2 shows the LRF versus radar reflectivity chart for WSI data at the :30 nominal time and the five available warm seasons (1997-2001). The LRF profile to 64 dBZ is consistent with that found in Reap and MacGorman (1989), but the steep LRF drop-off thereafter is unexpected. From Table 3, note that the number of cases also drops very sharply for very high reflectivities, which is expected. Corresponding LRF charts for the :00, :15, and :45 WSI nominal times (not shown) were similar to that in Fig. 2, as were those for the cool season.
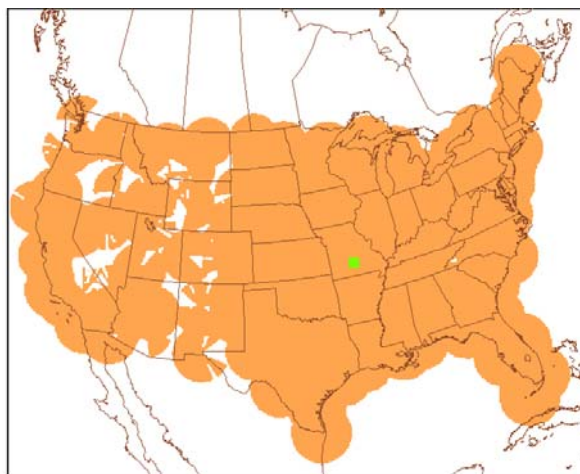
Figure. 1. Composite contiguous US coverage (orange shading) of WSR-88D network radars. The coverage umbrella of each radar is to 230 km, except for locations of substantial terrain occultation in western states. The small green-shaded square in the central US illustrates the size of a 10 x 10 array of the 10-km WSI/RCM gridboxes.

The corresponding LRF versus RCM reflectivity chart is shown in Fig. 3, based on the :15 nominal time and the 2002-03 warm seasons. This LRF profile does not exhibit the high reflectivity drop-off seen in Fig. 2, but the lack of reflectivity resolution beyond 55 dBZ could hide such a feature. As for the WSI data, the RCM relationships at :45 and the cool season were similar to that seen here.
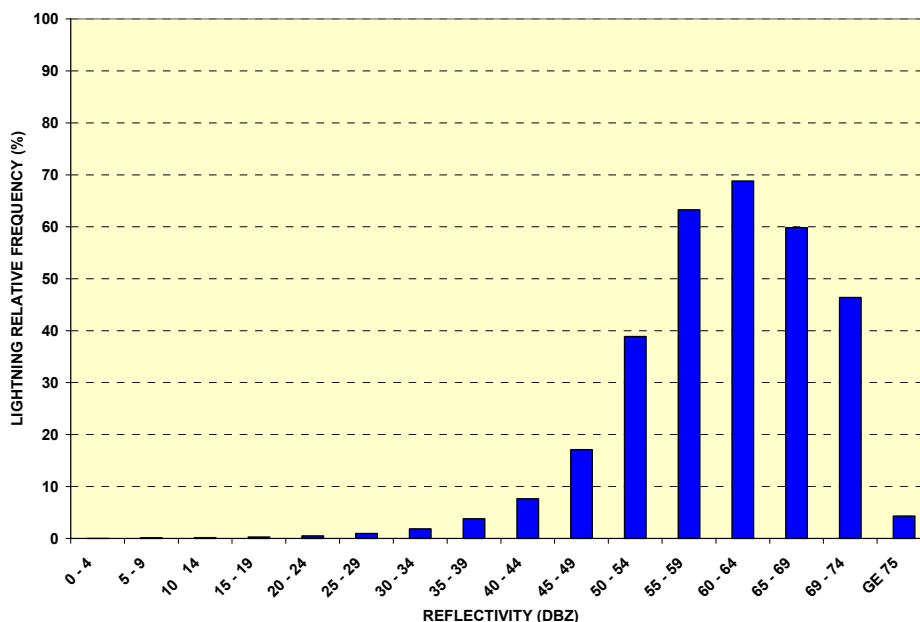
Figure 2. Lightning relative frequency versus WSI reflectivity. The data are from the CONUS, the 1997-2001 warm season (April – September) months, and all clock hours. The radar data have a nominal time of :30 and the lightning reports are valid :20 - :35 (times are minutes past the hour)

Table 3. Distribution of cases corresponding to Fig. 2. The right-hand column is the percentage of cases among all intervals beginning with 5 – 9 dBZ.

Reflectivity (dBZ)	Cases	Cases ≥ 5 dBZ (%)
0 – 4	1,703,663,866	---------
5 – 9	24,172,410	11.0846
10 – 14	37,835,020	17.3497
15 – 19	34,727,258	15.9246
20 – 24	32,891,926	15.0830
25 – 29	28,106,828	12.8887
30 – 34	21,008,887	9.6339
35 – 39	16,059,841	7.3644
40 – 44	10,983,435	5.0366
45 – 49	6,893,959	3.1613
50 – 54	3,953,781	1.8131
55 – 59	1,196,735	0.5488
60 – 64	212,396	0.0974
65 – 69	26,333	0.0121
70 – 74	2,731	0.0012
≥ 75	1,270	0.0005
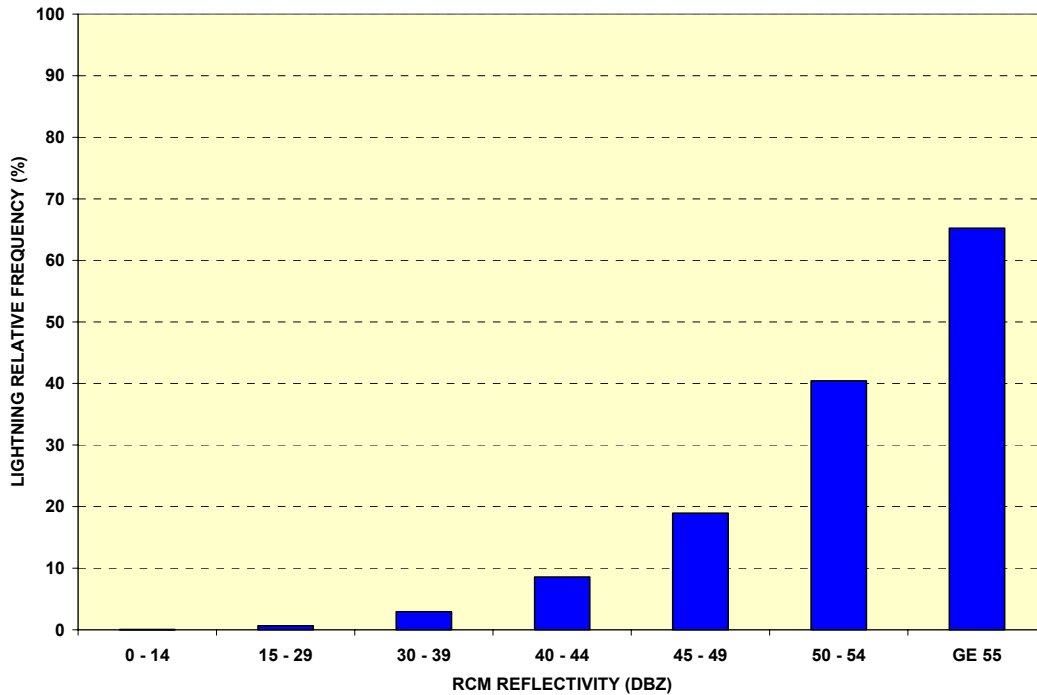
Figure 3. Same as Fig. 2 for RCM reflectivities, the :15 radar nominal time, and the 2002-03 warm seasons.

3.2 Reflectivity Maps

The statistical indication of very intense, non-precipitation echoes in the WSI archive (Fig. 2) prompted a case study investigation. To aid in the selection of cases, the full WSI archive was scanned for instances of ≥ 75 dBZ reflectivties. For each occurrence, the date, location, and the number of CTG lightning strikes for the concurrent 15-min period (defined above) were printed out for examination. The RCM data were also subjected to such an examination, but it was more cumbersome because of the large number of events in the broad ≥ 55 dBZ (peak) reflectivity interval.

A large number of dates (about 75) were selected for plotting and inspection of reflectivity maps. Most maps involved the presence of ≥ 75 dBZ (≥ 55 dBZ for RCM data) echoes without concurrent CTG lightning, but some of these events were intentionally chosen to include lightning. From this investigation, three types (or classes) of intense "false echoes" were identified. The most glaring among these was radar test patterns (see Fig. 4 for an example), which were found only in the WSI data. At least five grids with this type of contamination, which account for a large fraction of the ≥ 75 dBZ cases in Table 3, were included in the five warm seasons.
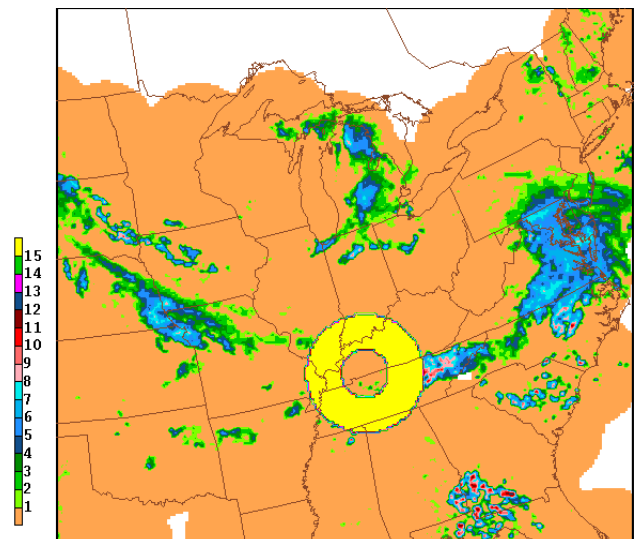
Figure 4. WSI reflectivity for 1845 GMT, 21 April 1997. The reflectivity categories are defined in Table 1. The ≥ 75 dBZ test pattern is from the Ft. Cambell, KY WSR-88D site.

Another class of suspect intense echoes was characterized by extreme reflectivity fluctuations in otherwise "normal" echo patterns. Many of the cases did not involve lightning or significant precipitation (based on a check of rain gage observa-

5

tions). However, a subset of the temporally-discontinuous events included CTG lightning, even to moderate intensity. Such an event is shown in Fig. 5, which involved a long-lived squall line in central and northern Texas. In this case, the core reflectivities in the line abruptly fluctuated between a base level of 50-59 dBZ (WSI categories 10-11), as in Fig. 5a, to the extreme level of ≥ 75 dBZ (WSI category 15) 15 min later, as in Fig. 5b. In this case, such reflectivity fluctuations continued back
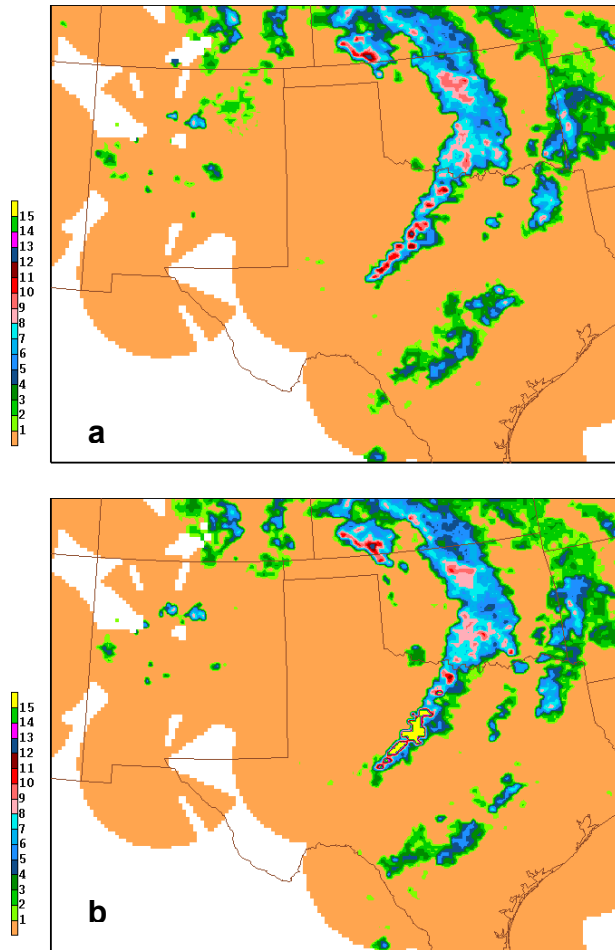
Figure 5. WSI reflectivity for (a) 0200 GMT and (b) 0215 GMT, 23 April 2000. The reflectivity categories are defined in Table 1. The abrupt increase in reflectivity seen in (b) was not associated with a corresponding increase in the CTG lightning rate.

and forth for two hours. The reflectivity fluctuations appeared over a long span of the echo line (Fig. 5b), and they were not related to the rate/intensity of CTG lightning strikes (not shown), which was considered moderate over a several hour period. In fact, for the 6-h duration of the ma-

ture squall line the lightning intensity associated with reflectivities greater than 64 dBZ (> category 13) was lower than for reflectivities in the 55-64 dBZ (category 11-13) range. These properties suggest the ≥ 75 dBZ (category 15) reflectivities were not caused by precipitation (at least not in an exclusive sense). The causative mechanism may be AP embedded within the echo line.

An example RCM case that involved extreme reflectivity fluctuations without lightning or significant precipitation is shown in Fig. 6. This case was selected from six studied from the 2002-03
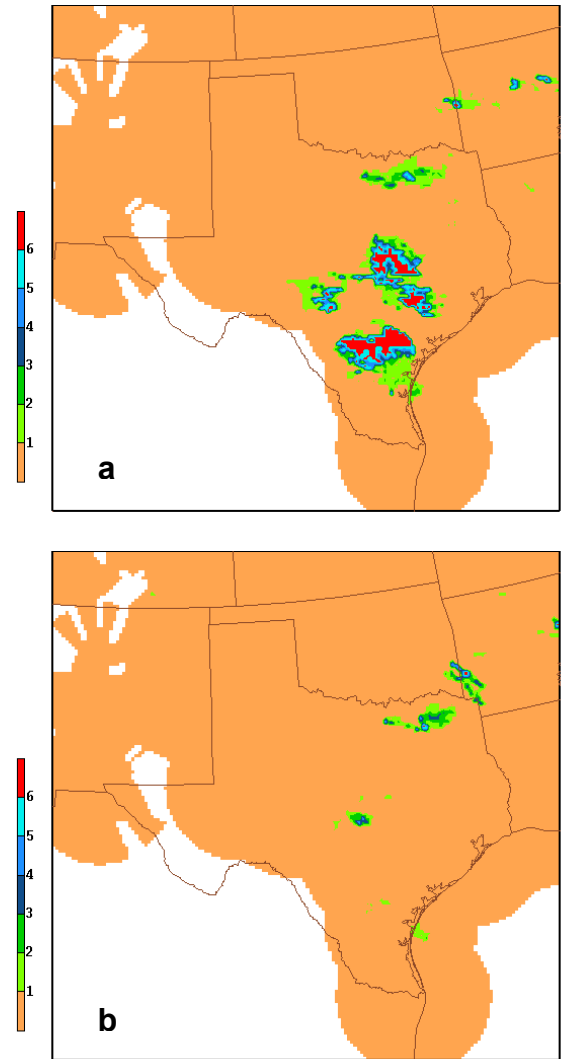
Figure 6. RCM reflectivity for (a) 0715 GMT and (b) 0815 GMT, 30 April 2002. CTG lightning or significant precipitation did not occur at either time. The reflectivity categories are defined in Table 1.

warm seasons. Note how the broad area of ≥ 50 dBZ reflectivities (RCM categories 5 - 6) at 0715 GMT on 30 April 2002 (Fig. 6a) completely disappeared within an hour later (Fig. 6b). AP is suspected as the cause of the false echoes in such cases--most occurred during nighttime or early morning hours, as for the case in Fig. 6.

A third class of false, intense (≥ 55 dBZ or ≥ 75 dBZ) echoes appeared as single gridbox reflectivity spikes (not shown). In the many cases falling in this class, the spike was surrounded by much lower reflectivity categories in some instances, and in others it was bounded by category 0. In most cases, the spikes appeared at favored locations within mountainous regions. In all cases, the reflectivity spike was not accompanied by CTG lightning.

3.3 Echo Climatology Maps

Echo climatology maps were derived from the WSI and RCM archives, as a different approach to investigate the presence of non-precipitation echoes. Warm and cool season echo relative frequency (ERF) maps were derived for each WSI and RCM reflectivity category, as well as for various ranges of the reflectivity categories. The object was to see whether suspected non-precipitation echoes are linked (statistically) to specific geographical locations.

The ERF maps revealed three types of data problems in the WSI and RCM archives. One problem was the finding of a substantial portion of 10-km gridboxes with category 1 or greater (≥ 5 dBZ) reflectivity in every case (i. e., 100% ERF), which is illustrated in Fig. 7 for the WSI warm season data. These gridboxes, which appear in locations beyond 230-km radar range or substantial terrain occultation, were distinguished by rather short samples. Note that the "true" radar coverage area shown in Fig. 1 does not include the 100% ERF areas in Fig. 7.
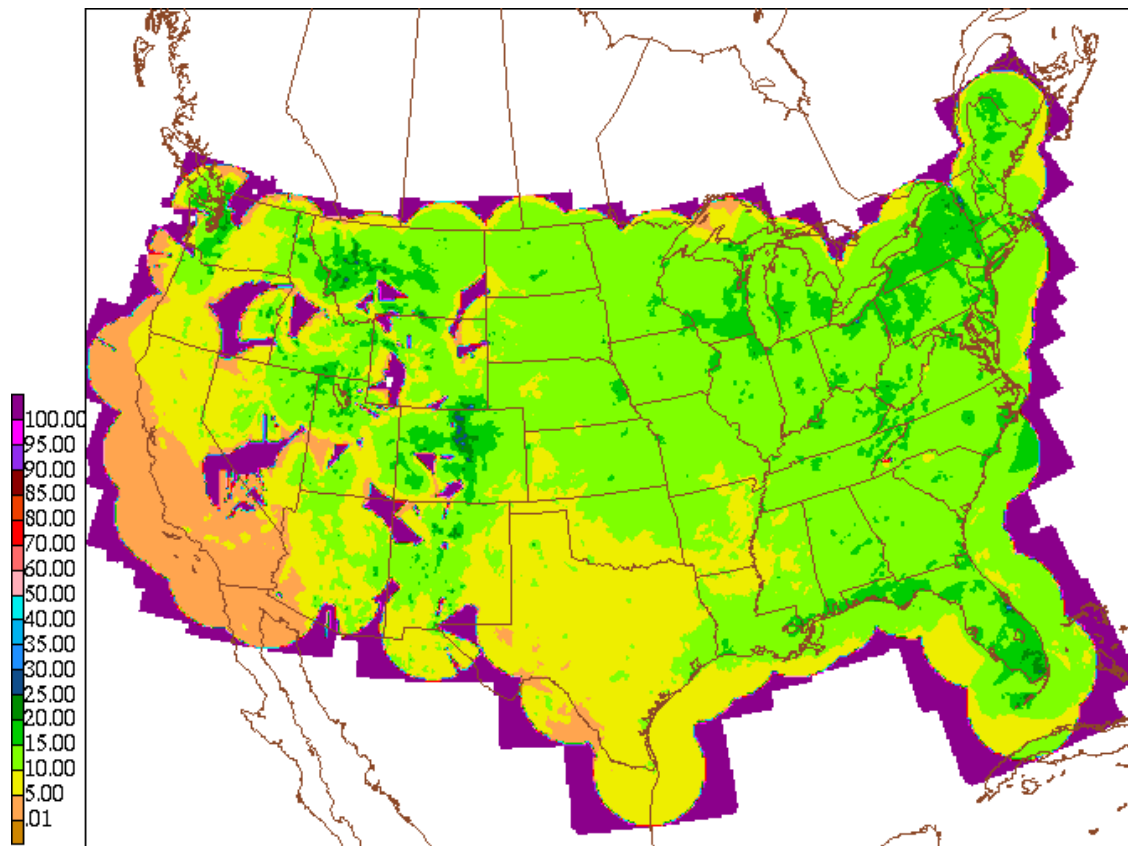
Figure 7. Warm season relative frequency of ≥ 5 dBZ WSI reflectivities in 10-km gridboxes. Relative frequencies of 100% appear for gridboxes beyond 230 km to the nearest radar and for gridboxes with substantial radar beam occultation.

In the case of the WSI data, the 100% ERF artifact was introduced during transferal of the reflectivities from the 2-km grid to the 10-km grid (see section 2). In the case of the RCM data, the number of gridboxes involved was far less, as reflectivities for gridboxes beyond 230-km range were set to missing previously during generation of the national mosaic (Kitzmiller et al. 2002). The problem still exists for a smaller subset, because non-zero

reflectivities in gridboxes with terrain occultation were retained.

Another problem was the appearance of small spurious ERF peaks in the upper reflectivity categories, which again was more prevalent for the WSI data. The warm season spurious peaks for the WSI data, based on ≥ 50 dBZ reflectivities, appear as small red spots in Fig. 8. Note that these spots appear most often in geographical
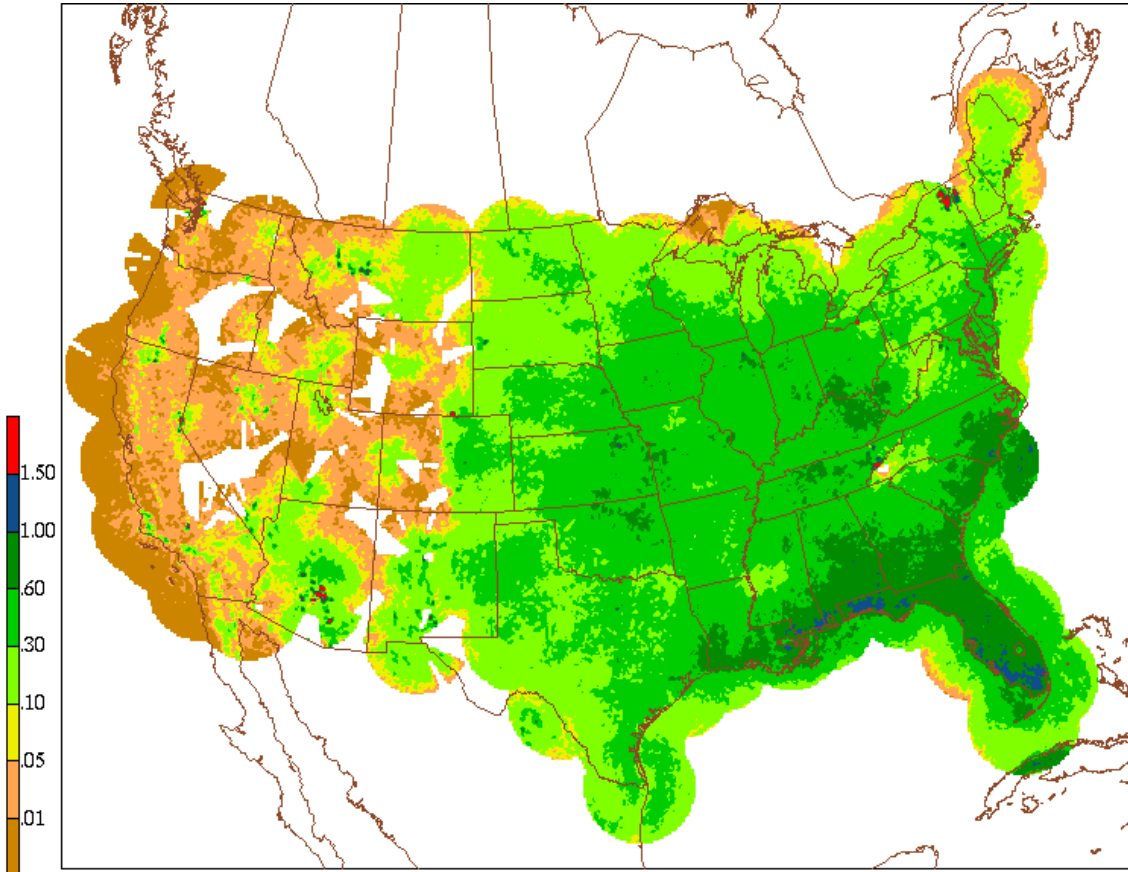
Figure 8. Warm season relative frequency (%) of WSI reflectivities of ≥ 50 dBZ after application of the first screening procedure. The sample consists of all :30 radar nominal times and the April – September months of 1997 - 2001. The small red spots depict spurious frequency peaks.

locations with rugged mountainous terrain. Similar spurious peaks also appeared for reflectivities in the mid-range, while a third type appeared for quite low reflectivities immediately around the radar sites (indicative of occasional ground clutter or other occasional low-level non-precipitation echoes).

It is important to note that corresponding maps of CTG lightning relative frequency, developed to

"match" the radar nominal times (not shown), contained no evidence to support the spurious ERF peaks. This finding, together with the finding noted in section 3.2 that CTG lightning did not accompany reflectivity spikes in the individual cases, suggests AP echoes as their causative mechanism.

A third problem seen in the ERF maps was strong evidence of radar beam overshooting of precipitation. This problem is indicated by the an-

omalously low ERFs (orange and brown colors), which appear mostly in the western US, in Fig. 8. The problem is considered more fully in the following section.

4. PROCEDURES TO IMPROVE THE QUALITY OF THE REFLECTIVITIES

4.1 Initial Procedures

As the initial attempt to improve the veracity of reflectivities in the WSI and RCM archives, two serial procedures were developed and applied. The first procedure is a simple screen that removed (set to missing) reflectivities for gridboxes that were beyond 230-km range or that exhibited substantial terrain occultation (see section 3.3). These gridboxes, which exhibit 100% ERF values in Fig. 7, comprised 14.5% of the WSI gridboxes that contained non-missing data over at least part of the archive period. While this area fraction is not tiny, the corresponding fraction of non-missing WSI data discarded was very small because the sub-samples for these gridboxes were very short. For example, the latter fraction was just 0.71% at the :30 nominal time during the warm season. In the case of the RCM data, the fraction of gridboxes removed by the screen was smaller than for the WSI data because only terrain occultation was involved (section 3.3). This fraction, averaged over the two seasons (a very slight variation in the fractions over the two seasons may have been an artifact of the small samples involved), was only 3.8%. It should be noted that following application of this screen, the areal coverage of gridboxes with non-missing data, for both the WSI and RCM archives, is precisely that shown in Fig. 1.

The second serial procedure involved development and application of automated decision tree checking of high reflectivities in the individual grids. The checks involved the degree of spatial and temporal continuity in the grids, together with the degree of consistency with concurrent and antecedent CTG lightning strikes. The checks were more elaborate for the WSI data than for RCM data, which was possible because of the higher temporal and reflectivity resolution of the former.

A summary of the decision tree checks for the WSI and RCM reflectivity grids is provided in Table 4. Note that the checks for both the WSI and RCM data were restricted to reflectivities of 50 dBZ and higher, which was due to the important role of CTG lightning strikes. The checks are directed primarily at the types of suspect echoes found in the case studies, as indicated by the descriptions in the table. Note also that the reflectivity category changes/adjustments for suspect echoes are simple when CTG lightning accompanies the echoes, but they involve alternative options when lightning is not present. Finally, although the checks-adjustments were developed largely on the basis of examinations of the WSI and RCM data for the warm season, they were not tailored for this season. Thus, they were applied to cool season data without change.

Statistical analyses of the computer output from the decision-tree checking runs revealed that the subset of reflectivities subjected to the checks constituted small fractions of the full warm and cool season samples of non-missing reflectivity values. Specifically, the $\geq$ 50 dBZ reflectivities subjected to scrutiny comprised only 0.29% (as an average) of the warm season WSI and RCM samples, and the percentage was even less for the cool season (0.07%). Also, among these reflectivities only 5.5% were changed for the WSI data, and an even smaller percentage (3.8%) was changed in the RCM data. Note that the differences in the percentages between the WSI and RCM data are not meaningful because the checks were different.

Following application of the two serial quality control (QC) procedures, the ERF maps were re-derived for evaluation of the benefit. In these maps, essentially no change in the spurious ERF features was found for reflectivity categories in the low and mid ranges, but for the $\geq$ 50 dBZ reflectivities subjected to the decision-tree checks the spurious peaks were reduced in size and magnitude. The latter is illustrated by comparing Fig. 9, which includes both serial procedures, with Fig. 8, which includes only the first screen. Note the shrinkage of the spurious ERF features (red spots) from Fig. 8 to Fig. 9.

It is noteworthy that while the spurious peaks were not fully removed for the broad $\geq$ 50 dBZ reflectivity interval underlying Figs. 8 and 9, they were fully removed for the more rare WSI reflectivities of 65 dBZ and above (not shown). The reason for the improved performance in the latter case is the decision tree checking for very high ($\geq$ 65 dBZ) reflectivities was more sophisticated than for 50 – 64 dBZ values. In particular, the checks and adjustments for $\geq$ 65 dBZ reflectivities involved not only lightning occurrence but also lightning intensity (Table 4).

Table 4.   Decision tree checks applied for (a) WSI and (b) RCM echo types, together with the concurrent cloud-to-ground lightning condition (left column).   Corresponding reflectivity category changes are listed in the right column. WSI and RCM reflectivity categories are defined in Table 1.

Echo type and lightning condition	Change in reflectivity category
(a) WSI	
≥ 75 dBZ "test pattern" without lightning	To missing
≥ 75 "echo spike" without lightning	To 0
≥ 75 dBZ echo with intense lightning	No change
≥ 65 dBZ echo with lightning	No change or change to slightly lower category according to lightning intensity
50 – 64 dBZ echo with lightning	No change
≥ 50 dBZ echo without lightning	No change, or change to slightly lower category for echoes with highly continuous spatial and temporal properties indicative of intense tropical rain, or --
	Change to lower category according to spatial and temporal continuity in the reflectivity and lightning patterns, or --
	Change to lower category or to missing (very rare)
(b) RCM	
≥ 55 dBZ "echo spike" without lightning	To 0
≥ 50 dBZ echo with lightning	No change
≥ 50 dBZ echo without lightning	No change, or change to slightly lower category for echoes with highly continuous spatial and temporal properties indicative of intense tropical rain, or --
	Change to category 3 when reflectivity pattern is spatially quasi-constant and temporally discontinuous, or --
	Change to lower category according to spatial and temporal properties of the reflectivity and lightning patterns
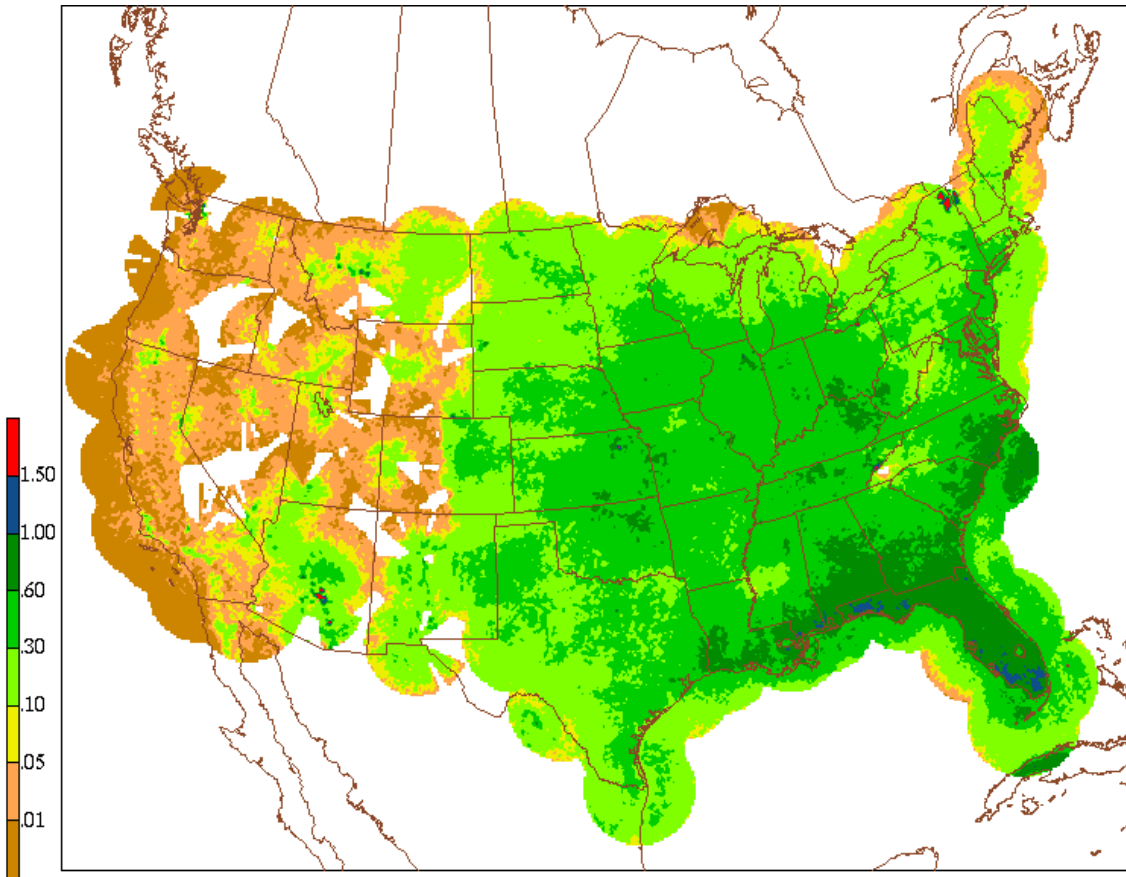
Figure 9. Same as Fig. 8, except with the inclusion of the decision-tree reflectivity checking (second QC procedure).

4.2 Final Procedure

Several concerns remained following application of the two QC procedures discussed above. First, they did not fully remove spurious ERFs for ≥ 50 dBZ reflectivities. Second, the screens do not apply to reflectivity categories in the low- to mid-range, which means that spurious ERF peaks previously noted for such reflectvities were not dealt with. Third, they do not address anomalously low ERFs, which were also noted above. Therefore, a final "catch-all" screening procedure was developed, which deals with anomalous ERFs over the full reflectivity range. The screen was developed by first identifying a fixed subset of gridboxes with suspect ERF values for one or more reflectivity categories. The screen was then applied by removing the reflectivities for the subset for each archived (or real time) grid.

The identification of anomalous ERF values in the maps was essentially subjective. It involved careful study of the maps to make judgments about whether or not the various features are realistic. Gridboxes where the ERFs were not considered valid were saved for subsequent removal of the reflectivities in each grid. It is noted that the grid-box identification process was greatly aided by importing the ERF grids into a geographical information system, where the ERF maps are displayed and the suspect gridboxes are identified and saved.

It is important to note that the judgment about whether or not to remove or retain a suspect ERF feature took into consideration the intended application of the reflectivities. In particular, for the LAMP thunderstorm predictor application, higher reflectivities are considered more important than lower values, and there is a need to minimize the number of gridboxes removed. Thus, the degree of thoroughness of removal of the spurious ERF by the screen was directly proportional to the nominal reflectivity category at which it appeared.

11

The full spectrum of suspect WSI, warm season ERF features removed by the screen is illustrated in Fig. 10. The figure shows the ERF field for ≥ 40 dBZ reflectivities before (10a) and after (10b) application of the final screen. The small red spots in 10a depict spurious ERF peaks, which not only include those for high reflectivities (Fig. 8), but they are also representative of those for reflectivities in the low and mid-ranges. Note that these spots are eliminated in 10b.
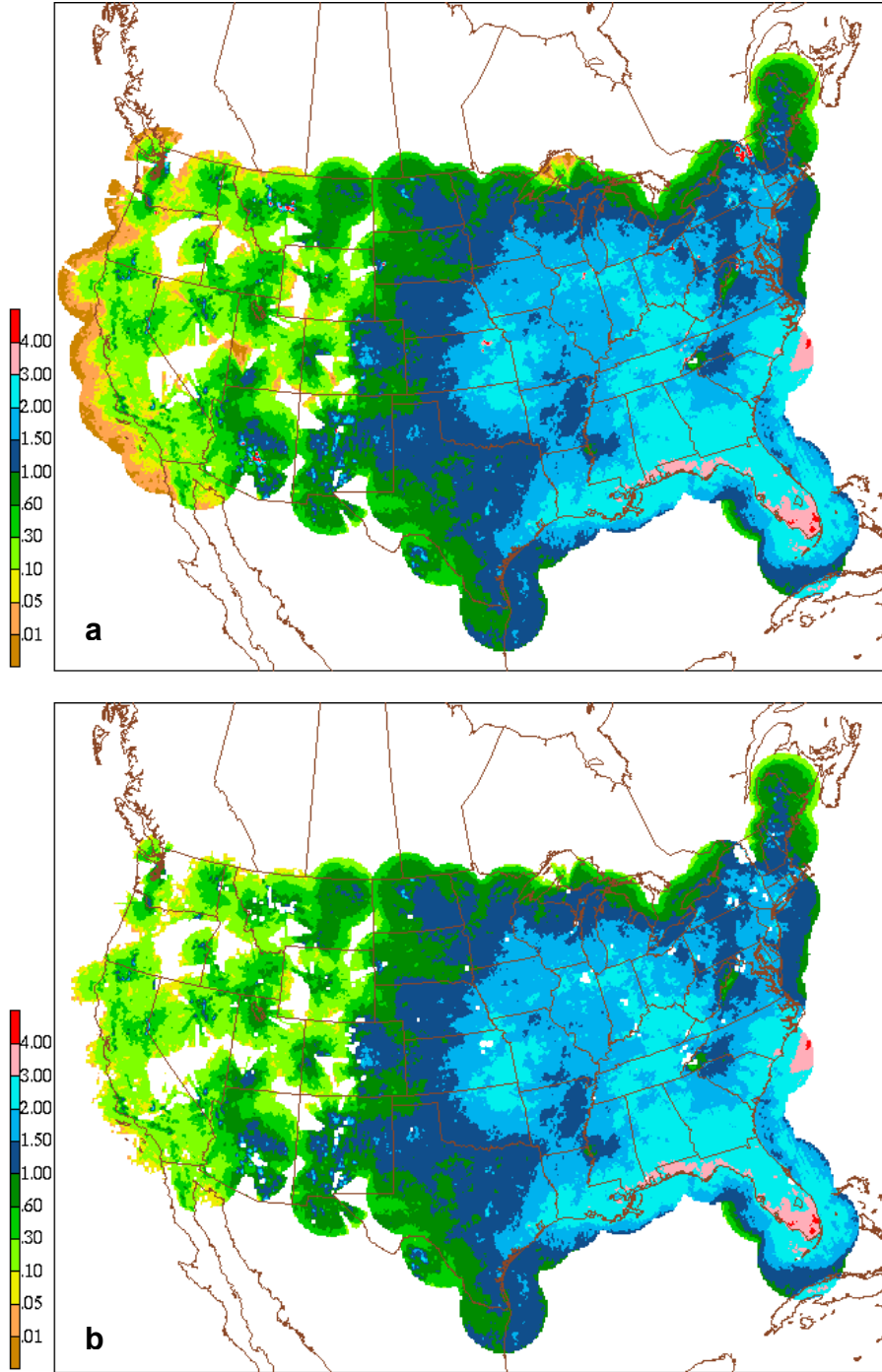
Figure 10. Warm season echo relative frequency (%) for WSI reflectivities of ≥ 40 dBZ before (a) and after (b) application of the final screen.

The removal of unrealistic ERFs in Fig.10b also includes those that were anomalously low in 10a. In 10a, areas off the West Coast, the intermountain West, and northern Lake Superior (highlighted by orange and brown colors) exhibit ≥ 40 dBZ ERFs that are much lower than prevailing values for neighboring areas. Note that these unrealistic ERFs generally appear at long radar range, but this is not always true in the intermountain western states. As noted previously, these non-representative ERFs are quite likely due to radar beam overshooting of precipitation, which generally increases with radar range. The problem is far more serious for the cool season, as indicated in Fig. 11. In this ERF map, which applies to ≥ 30 dBZ reflectivities following the final screen, thin bands of anomalously low values were allowed to remain after extensive areas were removed. A more complete elimination of the unrealistic ERFs was not performed because the resulting data loss would have been excessive for the LAMP application.
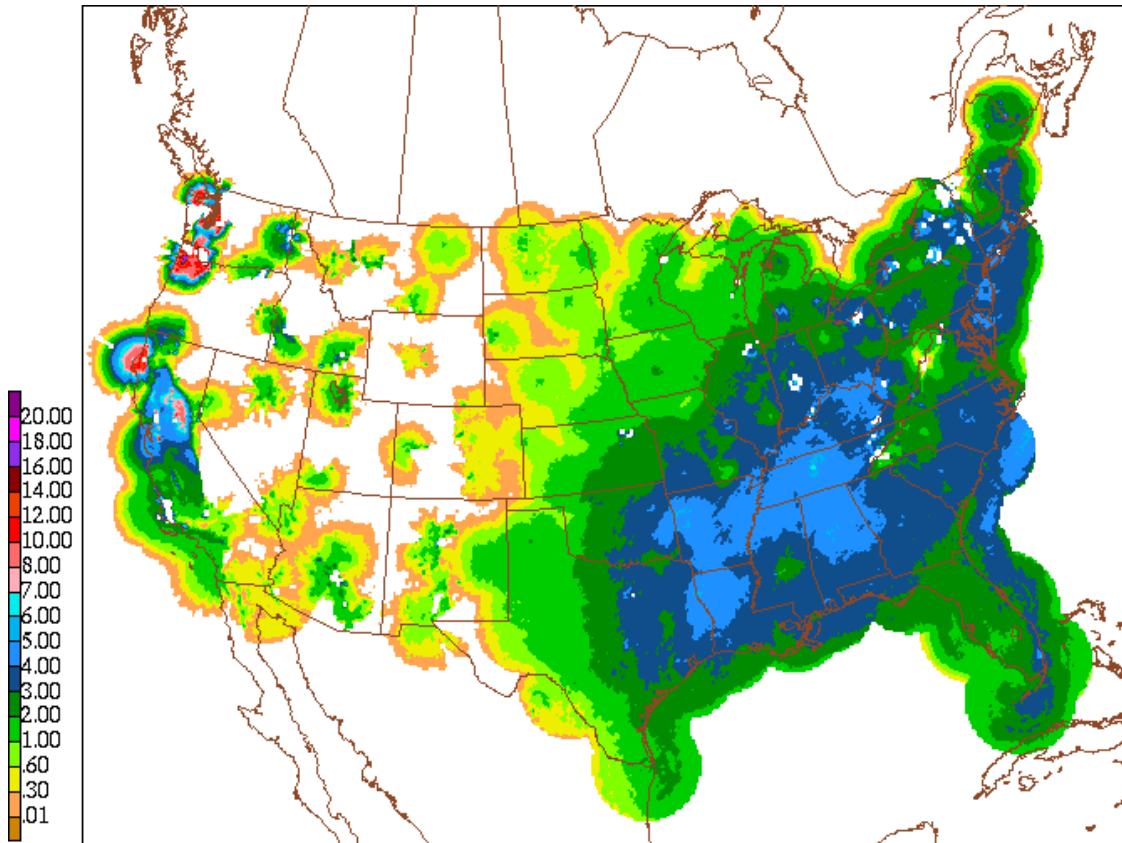
Figure 11. Cool season echo relative frequency (%) for WSI reflectivities of ≥ 30 dBZ following application of all QC procedures.

It is worthy to mention the fractions of the full WSI and RCM samples discarded by the final screen. For the WSI data, 3.9% and 10.6% of the CONUS warm and cool season samples, respectively, were thrown out by it. For the RCM data the corresponding fractions were 2.3% and 10.8%. Recall from section 4.1 that just 0.71% of the full WSI warm season sample was removed by the first screening procedure. Thus, while the volume of data removed by the final screen was not large, it was roughly an order of magnitude greater than that from the first screen. Note also that most of the discarded data were from the western US (Figs. 10b and 11), and the volume discarded for the cool season was roughly three times that for the warm season.

5. RESULTS AND DISCUSSION

In the previous section, the application of the three radar quality control (QC) procedures for echo climatology maps was demonstrated. In this section, similar examinations for the LRF profiles and example reflectivity maps discussed in section 3 are presented.

Fig. 12 shows LRF versus radar reflectivity charts following application of all QC procedures for the WSI and RCM data. A comparison of Fig. 12a with Fig. 2 reveals a remarkable improvement in the WSI LRF profile for ≥ 55 dBZ reflectivities, especially for extreme reflectivities of ≥ 65 dBZ. The corresponding comparison for the RCM data (Fig. 12 b and Fig. 3) indicates only a modest improvement, but the coarse reflectivity resolution precludes a commensurate assessment of the improvement. Similar examinations for other radar nominal times and the cool season yielded essentially the same findings.

It is worth pointing out that the WSI and RCM LRF profiles, such as those in Fig. 12, were essentially unaffected by the first and last screening processes. This result demonstrates that the improvement in the profiles resulted solely from application of the decision-tree checking process (the second serial procedure). The result is also consistent with the finding noted in section 4.1 that spurious ERFs for very high WSI reflectivites were fully eliminated by this procedure. Finally, the finding is also consistent with the fact the first and last screening processes are ignorant of the degree to which CTG lightning strikes were present in the discarded reflectivity data.

Re-examinations of the example reflectivity maps following application of the three QC procedures revealed the screens were effective in removing or adjusting the suspicious reflectivity features. Also, the maps also show how improvements in the suspect echo patterns resulted exclusively from the decision tree screening-adjustment process. In particular, this process was responsible for replacing most of the radar test pattern in Fig. 4 with missing values, as shown in Fig. 13. The small areas in the southern portion of the "doughnut" pattern that were replaced with upper WSI reflectivity categories were locations where CTG lightning occurred with spatially varying intensities.

In Fig. 14, we see how the decision tree process fully eliminated the questioned reflectivity jump seen in Fig 5. With the downward adjustment of suspect ≥ 65 dBZ (WSI category 13-15) reflectivities in Fig. 5b, reflectivities in the echo line are now consistent with those observed 15 min earlier (Fig. 14). As for the previous case, the CTG lightning rates were responsible for the reflectivity adjustments. On close inspection of Fig. 5b and 14b, it can be seen that ≥ 75 dBZ (category 15) reflectivites for two gridboxes in the echo line were changed to missing. This change is actually identical to that performed for the ≥ 75 dBZ test pattern in the previous case, as lightning did not occur in the two gridboxes.

A comparison of Figs. 6 and 15 shows how intense, presumed AP echoes in 6a were treated by the RCM decision-tree process. Note the questioned category 5 (50 – 54 dBZ) and 6 (≥ 55 dBZ) echoes in Fig. 6a were changed to category 3 (40 – 44 dBZ) in Fig. 15a, as no lightning (nor significant precipitation) was reported for the echo feature. Actually, for cases such as this, a reflectivity change to missing or to a RCM category lower than 3 would have been preferred, but either of these choices was thought to have greater negative consequences for the LAMP predictor application. This case, again, illustrates the QC limitations imposed by the coarse reflectivity and temporal resolution of the RCM data.
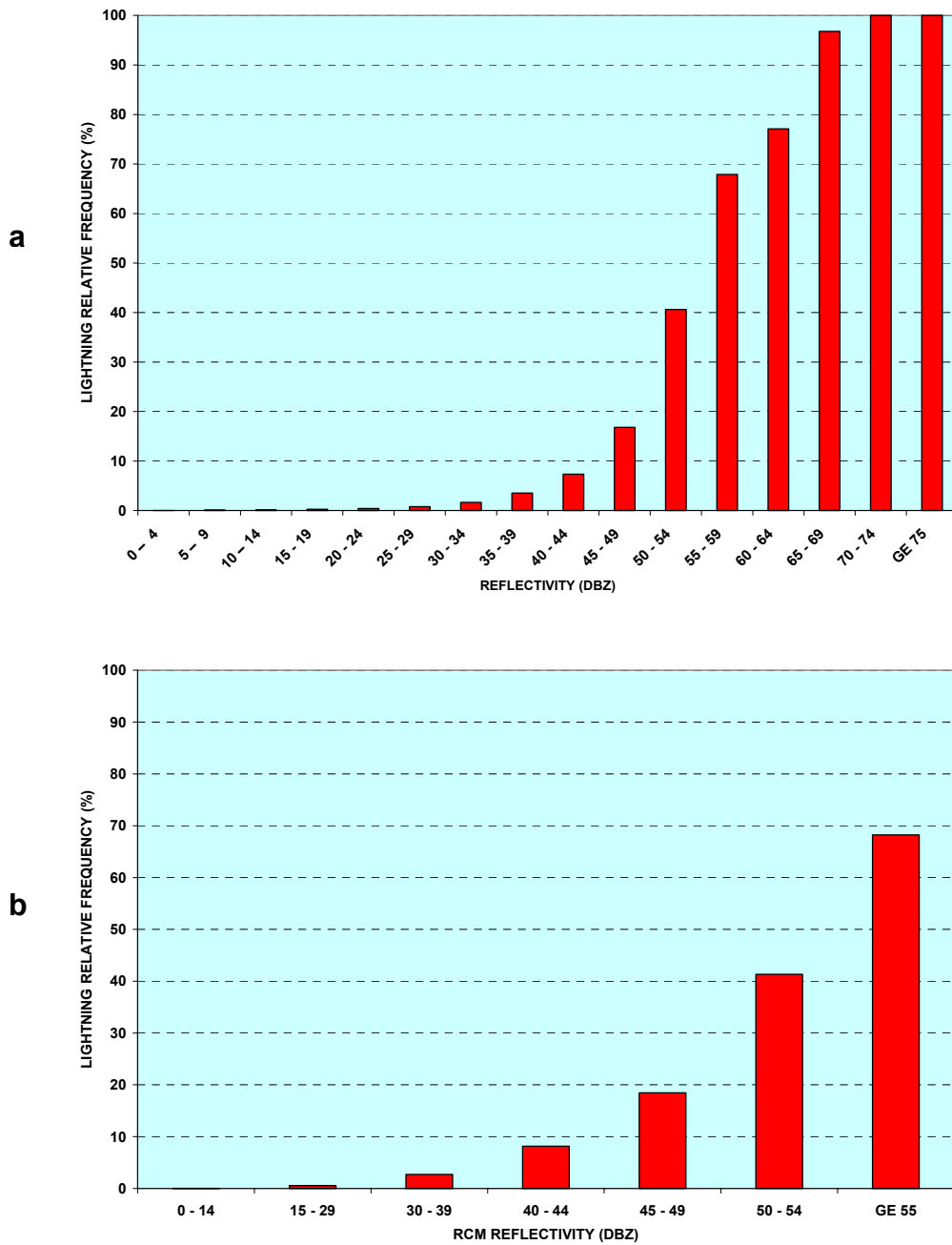
Figure 12. Same as Fig. 2 (a) and Fig. 3 (b) following application of all quality control procedures.
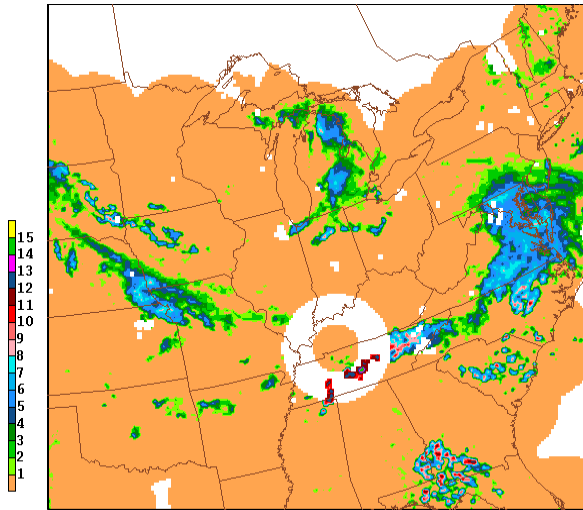
Figure 13 . Same as Fig. 4, except following application of all WSI quality control processes.
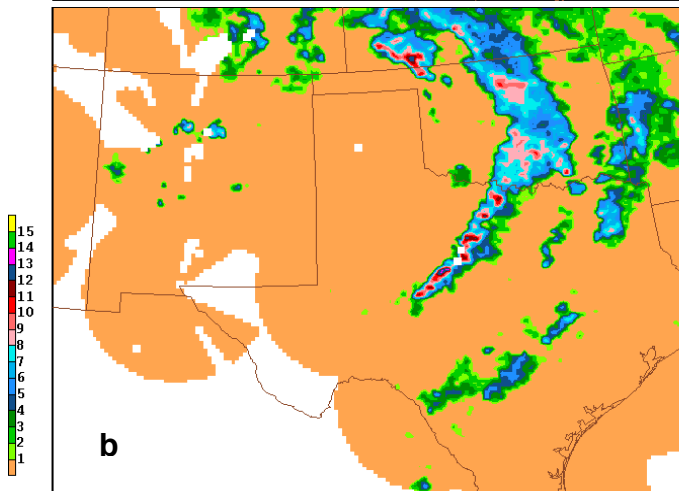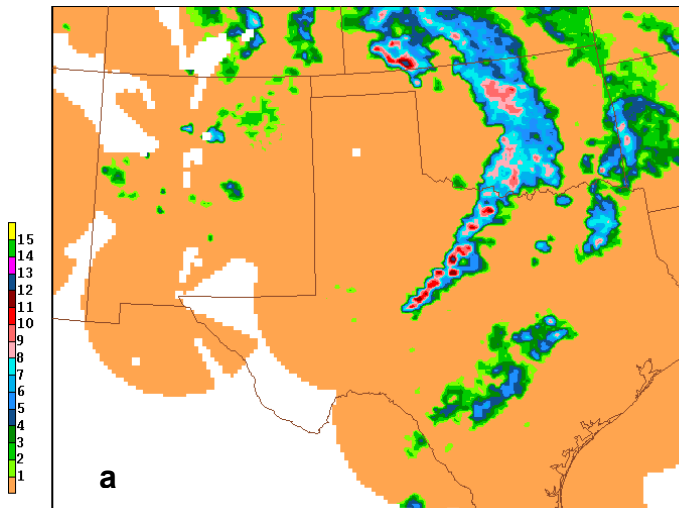
Figure 14. Same as Fig. 5, except following application of all WSI quality control processes.
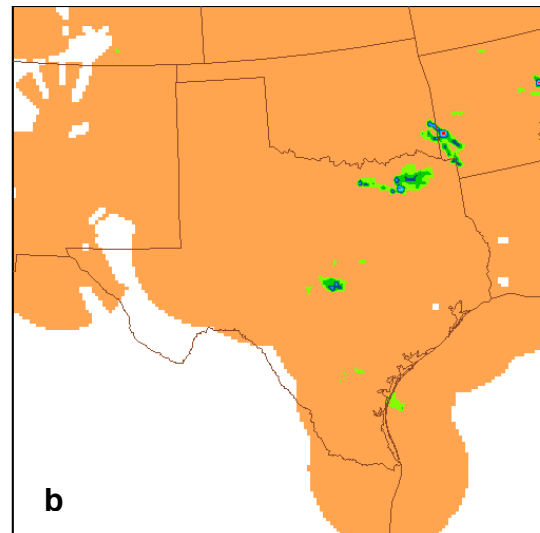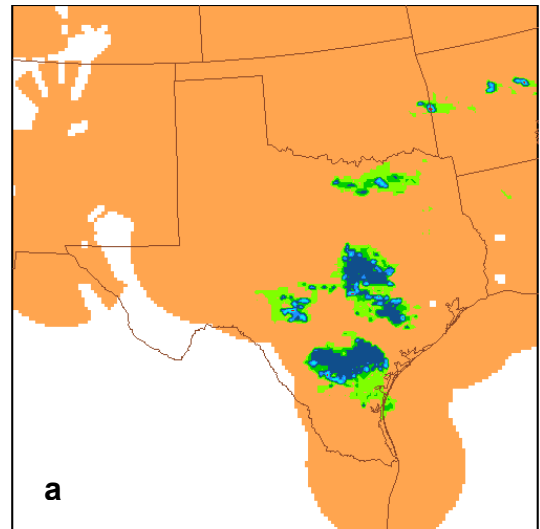
Figure 15. Same as Fig. 6, except following application of all RCM quality control processes.

A general comment concerning the three QC procedures is in order. We have noted, in this section and the previous one, that the serial QC procedures took into account the LAMP application of the reflectivity data. Specifically, the degree of removal of the anomalous ERFs took into consideration the volume of data loss, and the adjustment of one type of suspect RCM echo was slightly different than preferred. Recall that the precise choices in these two instances were influenced by the LAMP application, but only to a very slight degree. Thus, the three QC procedures are considered valid for other applications of the WSI and RCM data.

6. CONCLUSIONS, FINDINGS, AND COMMENTS

This study yielded the following conclusions and findings:

(1) The original 10-km WSI and RCM reflectivity grids were found to have good overall quality. This conclusion is based largely on the small fraction (about 5%) of ≥ 50 dBZ cases that were considered incorrect and changed by the decision tree checking process (second of the three serial QC processes applied.

(2) Significant fractions (~ 2 – 11%) of the CONUS WSI and RCM samples were discarded in the initial and final screens. Most of the discarded data was for the western states, and the data loss for the cool season was about three times that for the warm season.

(3) The application of the three serial QC procedures developed in this study appeared to result in a substantial improvement in the quality of the WSI and RCM data, especially for upper reflectivities in the WSI data.

(4) The improvement for the upper reflectivities was due essentially to the decision tree checking procedure.

(5) The decision tree checking procedure developed for the RCM data was substantially restricted by the coarse reflectivity and temporal resolution of the RCM data.

(6) The three serial QC processes should be valid for general applications of the WSI and RCM data.

Two comments are relevant to this study. First, as noted early in the article, the RCM data are presently the only source of timely, quality-controlled radar reflectivity data in the National Weather Service. Unfortunately, its coarse reflectivity and temporal resolution precluded the development of QC procedures with a level of sophistication commensurate to that for the WSI data. Further, because resolution consistency between the WSI and RCM data was a requirement for the LAMP thunderstorm application, the resolution short-coming of the RCM data limits the LAMP predictor utility of both data types. In effect, some of the benefit of the enhanced quality control processes for the WSI data was likely lost.

Another point concerns ground truth in automated quality control of radar reflectivity data. In this study, CTG lightning strike data were applied as ground truth for most precipitation echoes. While the study indicated a significant benefit of such ground truth for the QC of radar reflectivities, its limitations precluded development of more definitive procedures In future studies of this type, the incorporation of more comprehensive ground truth provided by cloud and precipitation information from satellite and raingage measurements should be attempted.

7. ACKNOWLEGEMENTS

8. REFERENCES

Charba, J. P., and F. Liang, 2005: Automated two-hour thunderstorm guidance forecasts. Preprints, *Conference on Meteorological Applications of Lightning Data.* San Diego, Amer. Meteor. Soc., CD-ROM **3.4**.

Cummins, K. L., M. J. Murphy, E. A. Bardo, W. L. Hiscox, R. B. Pyle, and A. E. Pifer, 1998. A combined TOA/MDF technology upgrade of the U. S. national lightning detection network, *J. Geophys. Res.*, **103**, 9035-9044.

Fread, D. L., R. C. Shedd, G. F. Smith, R. Farnsworth, C. N. Hoffeditz, L. A. Wenzel, S. M. Wiele, J. A. Smith, and G. H. Day, 1995: Modernization in the National Weather Service river and flood program. *Wea. Forecasting*, **10**, 477-484.

Fulton, R. A, J. P. Breidenbach, D. J. Seo, D. A. Miller, and T. O'Bannon, 1998: The WSR-88D rainfall algorithm. *Wea. Forecasting*, **13**, 377-395.

Ghirardelli, J., 2005: An overview of the redeveloped localized aviation mos program (LAMP) for short range forecasting. Preprints, *21st Conference on Weather Analysis and Forecasting*, Washington, DC, Amer. Meteor. Soc., Conference Paper No. **13.B5** (http://ams.confex.com/ams/WAFNWP34BC/techprogram/paper_95038.htm).

Idone, V. P., D. A. Davis, P. K. Moore, Y. Wang, R. W. Henderson, and P. F. Jamason, 1998a. Performance evaluation of the U. S. national lightning detection network in eastern New York: 1. Detection efficiency, *J. Geophys. Res.*, **103**, 9045-9056.

_____, 1998b. Performance evaluation of the U. S. national lightning detection network in eastern New York: 2. Location Accuracy, *J. Geophys. Res.*, **103**, 9057-9069.

Kitzmiller, D. H., F. G. Samplatsky, and D. L. Keller, 2002: Production of a national radar reflectivity mosaic and automated radar observations from WSR-88D radar coded messages. *NOAA Tech. Memo.* NWS MDL 83, National Oceanic and Atmospheric Administration, U.S. Department of Commerce, 23 pp.

OFCM, 1991: Doppler radar meteorological observations: Part C, WSR-88D products and algorithms. Federal Meteorological Handbook 11, FMC-H11C-1991, Office of the Federal Coordinator for Meteorological Services and Supporting Research, Silver Spring, MD, 210 pp.

Reap, R. M., and D. R. MacGorman, 1989: Cloud-to-ground lightning: Climatological characteristics and relationships to model fields, radar observations, and severe local storms. *Mon. Wea. Rev.*, **117**, 518–535.